

Deutscher Wetterdienst
Wetter und Klima aus einer Hand



ESA Cloud_cci

Algorithm Theoretical Baseline Document v6.2

(Applicable to Cloud_cci version 3.0 products)



Issue 6 Revision 2

14 October 2019

Deliverable No.: D-2.1


ESRIN/Contract No.: 4000109870/13/I-NB

Project Coordinator: Dr. Rainer Hollmann
Deutscher Wetterdienst
rainer.hollmann@dwd.de

Technical Officer: Dr. Simon Pinnock
European Space Agency
Simon.Pinnock@esa.int

DOIs of Cloud_cci datasets: DOI: [10.5676/DWD/ESA_Cloud_cci/AVHRR-PM/V003](https://doi.org/10.5676/DWD/ESA_Cloud_cci/AVHRR-PM/V003)
DOI: [10.5676/DWD/ESA_Cloud_cci/AVHRR-AM/V003](https://doi.org/10.5676/DWD/ESA_Cloud_cci/AVHRR-AM/V003)
DOI: [10.5676/DWD/ESA_Cloud_cci/ATSR2-AATSR/V003](https://doi.org/10.5676/DWD/ESA_Cloud_cci/ATSR2-AATSR/V003)



	Doc:	Cloud_cci_D2.1_ATBD_v6.2.doc			
	Date:	14 October 2019			
	Issue:	6	Revision:	2	Page 2

Document Change Record

Document, Version	Date	Changes	Originator
ATBD Version 5.1	12/09/2017	Released precursor version of ATBD applicable for Cloud_cci dataset version 2	M. Stengel
ATBD Version 6.0	30/10/2018	Revision wrt. this document representing algorithms (CC4CL) and Level 3 tools used for processing of AVHRR-AM/PMv3 and ATSR2-AATSRv3 datasets <ul style="list-style-type: none"> Updating Section 1, in particular sub section 1.2 and 1.3 to represent data set versions 3. Removing outdated information from Section 2 Updated Section 3: <ul style="list-style-type: none"> updated information on cloud detection and cloud phase adding subsection 3.4 on the calculation of broadband fluxes Adding Section 4.2.3 on the aggregation of broadband flux properties. 	M. Stengel
ATBD Version 6.1	05/02/2019	Updates after ESA review of document version 6.0. E.g.: <ul style="list-style-type: none"> Revising subsection 3.1 Minor edits to subsections 3.2 and 3.3 Minor updates to section 4 	M. Stengel
ATBD Version 6.2	12/03/2019	Updates after ESA review of document version 6.1.E.g. <ul style="list-style-type: none"> Adding a comment on BB flux uncertainties Adding Section 1.4 (copy/paste from PVIRv5) for consistency between ATBD, PUG, and PVIR 	M. Stengel

Purpose

The purpose of the Cloud_cci Algorithm Theoretical Baseline Documents (ATBDs) is to document the theoretical background of all components of the algorithms used for the generation of the Cloud_cci cloud property datasets v3.0. This document focusses on overarching aspects as individual, in-depth ATBDs exist for the two retrieval system Community Cloud retrieval for Climate (CC4CL, [ATBD-CC4CLv6](#)).



	Doc:	Cloud_cci_D2.1_ATBD_v6.2.doc			
	Date:	14 October 2019			
	Issue:	6	Revision:	2	Page 3

Table of Contents

1.	Introduction	4
1.1	The ESA Cloud_cci project.....	4
1.2	The Cloud_cci version 3 datasets	5
1.3	Cloud_cci cloud products.....	7
1.4	Uncertainties	9
2.	Satellite sensors and their measurement records	11
2.1	AVHRR.....	11
2.2	AATSR	13
2.3	Limitations of the (inter-)calibration	15
3.	The Community Cloud retrieval for CLimate (CC4CL) retrieval system.....	16
3.1	Cloud detection	16
3.2	Cloud typing & phase	16
3.3	Optimal estimation retrieval of cloud properties.....	17
3.4	Calculation of the broadband fluxes	17
3.5	Limitations	17
4.	Generation of the Level-3 products.....	20
4.1	Level-3U products.....	20
4.2	Level-3C products.....	20
4.2.1	Aggregating cloud mask and phase information	20
4.2.2	Aggregating microphysical and macrophysical cloud properties	20
4.2.3	Aggregation of broadband fluxes.....	22
4.2.4	Limitations in the aggregation of Level-3 products.....	23
5.	References.....	24
6.	Glossary.....	27

	Doc:		Cloud_cci_D2.1_ATBD_v6.2.doc		
	Date:		14 October 2019		
	Issue:	6	Revision:	2	Page 4

1. Introduction

1.1 The ESA Cloud_cci project

The ESA Cloud_cci project covers the cloud component in the European Space Agency's (ESA) Climate Change Initiative (CCI) programme (Hollmann et al., 2013). In the ESA Cloud_cci project, long-term and coherent cloud property datasets have been generated exploiting the synergic capabilities of different Earth observation missions (European and non-European) allowing for improved accuracies and enhanced temporal and spatial sampling better than those provided by the single sources. The Cloud_cci datasets are the attempt to respond to GCOS requirements for the Cloud Properties Essential Climate Variable (ECV).

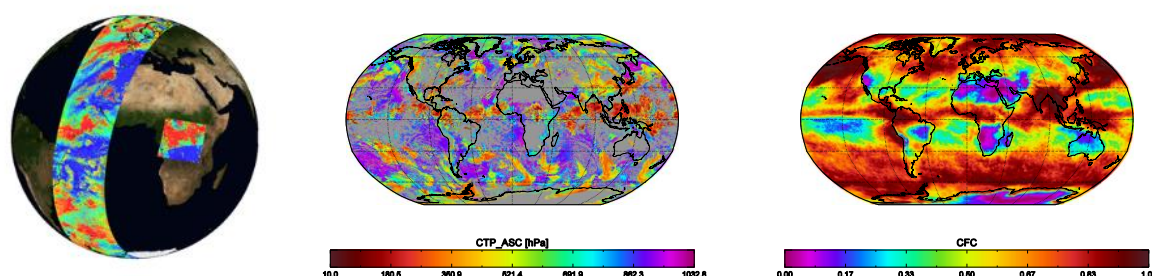



Figure 1-1 Examples of Cloud_cci cloud products. Left: Pixel-based (Level 2), middle: daily composite on a global grid (Level 3U), right: monthly averaged on a global grid (Level 3C)

To make the Cloud_cci datasets improved compared to existing ones, the following two essential steps were undertaken:

- 1) Revisit the measurement data (Level-1) and corresponding calibration performance and development of a carefully inter-calibrated and rigorously quality checked radiance data sets for AVHRR, so called Fundamental Climate Data Record (FCDR). Within this effort the calibration of AVHRR, MODIS and AATSR was compared and characterized. Please see the ATBDv5 for more information about all sensors used and their imaging characteristics. More information on the AVHRR FCDR produced and used is available in RAFCDRv1.0.
- 2) Development of two state-of-the-art physical retrieval systems that use the optimal estimation technique for a simultaneous, spectrally consistent retrieval of cloud properties including pixel-based uncertainty measures. The first retrieval framework is the Community Cloud retrieval for Climate (CC4CL; Sus et al., 2017; McGarragh et al., 2017) which is applied to AVHRR and AVHRR-heritage channels (i.e. channels which are available from all sensors) of MODIS and AATSR. The second retrieval framework is the Freie Universität Berlin AATSR MERIS Cloud retrieval (FAME-C; Carbajal Henken et al., 2014) and is applied to synergistic MERIS and AATSR measurements on-board of ENVISAT.

Based on these developments, six multi-annual, global datasets of cloud properties were generated using the passive imager satellite sensors AVHRR, MODIS, (A)ATSR and MERIS. These datasets were comprehensively evaluated (1) by using accurate reference observations of ground stations and space-based Lidar measurements and (2) by comparisons to existing and well-established global cloud property datasets. These datasets were published as **version 2** (version 1 being shorter, prototype datasets) and Digital Object Identifiers issued:

[DOI:10.5676/DWD/ESA_Cloud_cci/AVHRR-PM/V002](https://doi.org/10.5676/DWD/ESA_Cloud_cci/AVHRR-PM/V002)
[DOI:10.5676/DWD/ESA_Cloud_cci/AVHRR-AM/V002](https://doi.org/10.5676/DWD/ESA_Cloud_cci/AVHRR-AM/V002)
[DOI:10.5676/DWD/ESA_Cloud_cci/MODIS-Terra/V002](https://doi.org/10.5676/DWD/ESA_Cloud_cci/MODIS-Terra/V002)
[DOI:10.5676/DWD/ESA_Cloud_cci/MODIS-Aqua/V002](https://doi.org/10.5676/DWD/ESA_Cloud_cci/MODIS-Aqua/V002)
[DOI:10.5676/DWD/ESA_Cloud_cci/ATSR2-AATSR/V002](https://doi.org/10.5676/DWD/ESA_Cloud_cci/ATSR2-AATSR/V002)
[DOI:10.5676/DWD/ESA_Cloud_cci/MERIS+AATSR/V002](https://doi.org/10.5676/DWD/ESA_Cloud_cci/MERIS+AATSR/V002)

	Doc:	Cloud_cci_D2.1_ATBD_v6.2.doc			
	Date:	14 October 2019			
	Issue:	6	Revision:	2	Page 5

These datasets were comprehensively documented in [Stengel et al. \(2017\)](#), the Product Validation and Intercomparisons Report (PVIR; [PVIRv4.1](#)), the Product User Guide ([PUGv3.1](#)) and the overarching Algorithm Theoretical Baseline Document (ATBD, [ATBDv5](#)) together with specific ATBDs for FAME-C ([ATBD-FAME-Cv5](#)) and CC4CL ([ATBD-CC4CLv5](#)).

To facilitate a suitable application of Cloud_cci datasets for model evaluation, satellite simulators have been developed, tested and published ([Eliasson et al., 2019](#) and [Stengel et al., 2018](#)).

In addition to the datasets mentioned above, AVHRR and AATSR based datasets were reprocessed again building the **version 3.0 datasets**, based on an updated CC4CL, partly covering longer periods (AVHRR) and including an extended product portfolio by including shortwave and longwave, all-sky and clear-sky radiative flux properties and top and bottom of the atmosphere (TOA and BOA).

The remaining part of this document will exclusively focus on the algorithm version used for generation of the version 3 datasets. In addition to this ATBD, these v3 datasets are being documented in [PVIRv6.0](#), [PUGv5.0](#) and [Stengel et al. \(2019\)](#).

1.2 The Cloud_cci version 3 datasets

Three Cloud_cci version 3 cloud property datasets have been generated, based on AVHRR and ATSR2+AATSR, utilizing the AVHRR-heritage channels (0.6, 0.8, 1.6/3.7, 10.8, 12.0 μm) only. The retrieval system used was an updated version of CC4CL. Since AVHRR sensors were separated into morning and afternoon orbits. Figure 1-2 shows the temporal coverage of the v3 datasets.

Table 1-1 summarizes the algorithms, sensors and satellites used for each dataset. The official versions of the datasets, as released under the issued Digital Object Identifies (DOIs, see Table 1-1), do not contain any diurnal cycle or satellite drift correction. Potential methods for such a drift correction were investigated for AVHRR and were documented in [RODCv1.0](#). In Figure 1-3 the local observation time of each individual sensor considered are visualized. This information is often essential for properly characterizing time series of cloud properties derived from the satellite-based climate datasets. Other important aspects are the imaging properties. The sensors differ in terms of native footprint resolution (1x1km² for ATSR2, AATSR; 5x1km² for AVHRR GAC). This, together with the sensor swath width, leads to very different observation frequency and spatial coverage. While AVHRRs have a complete global coverage within a day, the AATSR sensor needs about 3 days to accomplish this, however, with a higher spatial resolution compared to AVHRR.

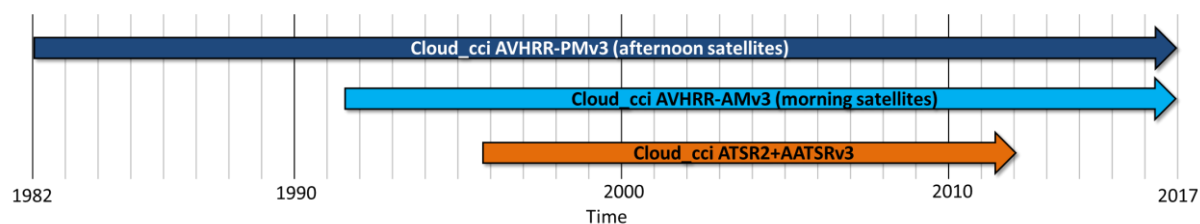



Figure 1-2 Overview of Cloud_cci v3 datasets and the time periods they cover.

All datasets contain identical sets of cloud properties: cloud mask/fraction (CMA/CFC), cloud phase/liquid cloud fraction (CPH), cloud top pressure/height/temperature (CTP/CTH/CTT), cloud effective radius (CER), cloud optical thickness (COT), spectral cloud albedo at two wave lengths (CLA) and liquid/ice water path (LWP/IWP). In addition a set of radiative broadband fluxes are contained: top of the atmosphere (TOA) and bottom of the atmosphere (BOA) radiative fluxes for shortwave and longwave, in clear-sky and all-sky conditions, upwelling and downwelling.

The data is presented at different processing levels ranging from pixel-based retrieval products (Level-2), which are additionally projected (sampling - no averaging) onto a global Latitude-

	Doc:	Cloud_cci_D2.1_ATBD_v6.2.doc			
	Date:	14 October 2019			
	Issue:	6	Revision:	2	Page 6

Longitude grid of 0.05° resolution (global composite, Level-3U), to monthly data summarizes including averages, standard deviation and histograms - all defined on a global Latitude-Longitude grid of 0.5° resolution (Level-3C). See Section 1.3 for more details.

All cloud properties are accompanied by uncertainty measures at all processing levels, which range from optimal estimation based uncertainty on pixel level (Level-2 and Level-3U) to propagated uncertainties in the monthly Level-3C products. See Section 1.4 for more information. Level-2 uncertainties exist also for the radiative broadband flux properties (See ATBD-CC4CL_TOA_FLUXv1.1), but are only included in the ATSR2-AATSRv3 dataset.

Key strengths of Cloud_cci version 3 datasets:

- The Cloud_cci datasets are based on a state-of-the art retrieval systems named CC4CL that uses the optimal estimation (OE) technique and are applied to passive imager sensors of current and past European and non-European satellite missions.
- All v3 datasets contain consistent sets of cloud and radiative flux properties.
- The measurement records of the utilized sensors have been revisited, re-characterized and, in case of AVHRR, re-calibrated.
- One special feature of CC4CL is, among others, its applicability to multiple sensors: ATSR2, AATSR, MODIS, AVHRR (and other passive imaging sensors) down to spatial footprint resolutions of 1km.
- Radiative consistency of derived cloud parameters is achieved by the OE-based, iterative fitting of a physically consistent cloud model (and radiative transfer simulations therefrom) to the sensor measurements in the visible and thermal infrared spectral range.
- Pixel-level uncertainty characterization is facilitated by the OE technique, which is physically consistent (1) with the uncertainties of the input data (e.g. measurements, a-priori) and (2) among the retrieved variables. These pixel-level uncertainties are further propagated into the monthly products using a developed sound mathematical framework.
- Potential to combine AVHRR-heritage datasets to achieve increased temporal resolution by including multiple polar-orbiting satellite instruments, which also allows for mature cloud property histograms on 0.5° resolution due to highly increased sampling rate.
- Comprehensive assessment and documentation of the retrieval schemes and the derived cloud property datasets, including possibilities of drift- and diurnal cycle corrections.
- Availability of a developed Cloud_cci satellite simulator facilitating the applicability of Cloud_cci data in regional and global climate models evaluation efforts.
- All datasets are available in netcdf (v4) format and fulfil high CCI-internal and external data standards (e.g. Climate and Forecast - CF conventions).

Table 1-1 *Cloud_cci v3 datasets with the algorithms, sensor(s) and satellite(s) used and the time periods they cover. The Digital Object Identifiers (DOI) of all datasets are also listed.*

Dataset name	Sensor(s)	Satellite(s)	Time period	Algorithm
Cloud_cci AVHRR-PM DOI:10.5676/DWD/ESA_Cloud_cci/AVHRR-PM/V003	AVHRR-2/-3	NOAA-7, -9, -11, -14, -16, -18, -19	1982-2016	CC4CL
Cloud_cci AVHRR-AM DOI:10.5676/DWD/ESA_Cloud_cci/AVHRR-AM/V003	AVHRR-2/-3	NOAA-12, -15, -17, Metop-A	1991-2016	CC4CL
Cloud_cci ATSR2-AATSR DOI:10.5676/DWD/ESA_Cloud_cci/ATSR2-AATSR/V003	ATSR2, AATSR	ERS2, ENVISAT	1995-2012	CC4CL

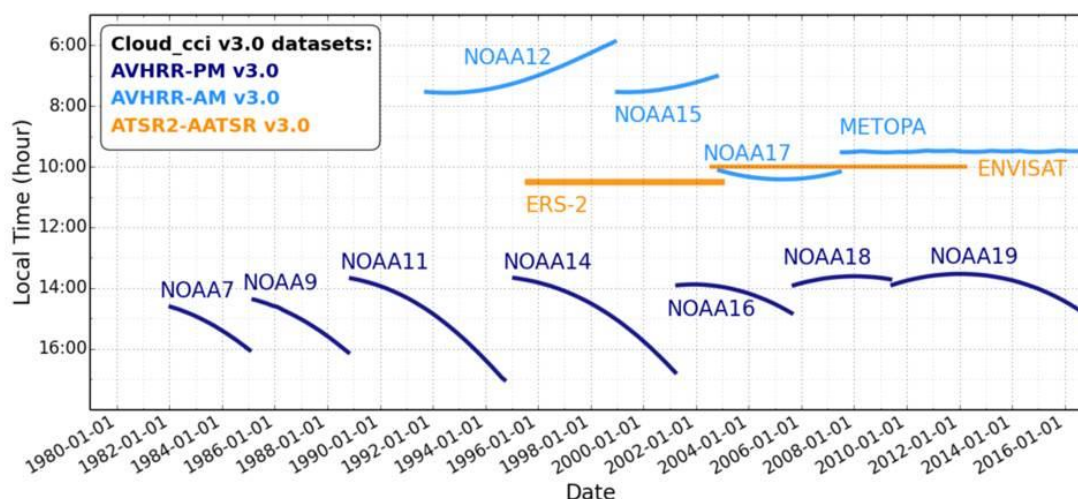


Figure 1-3 Time periods and local observation times (equator crossing times) of each satellite sensor considered in Cloud_cci. Figure is taken from [Stengel et al. \(2019\)](#).

1.3 Cloud_cci cloud products


The cloud properties derived on pixel level of each utilized sensor are listed in Table 1-2. It is important to note that the cloud properties CLA, LWP, IWP are not directly retrieved, but rather determined from retrieved COT and CER in a post processing step. The same applies to CTH and CTT, which are inferred from the retrieved CTP. In addition, it needs to be noted that for the determination of radiative fluxes a fair amount of ERA-Interim data was required.

Based on the pixel level retrievals the data is further processed into different processing levels as summarized in Table 1-3. Level-3U denotes a global composite on a global Latitude-Longitude grid (of 0.05° resolution) onto which the Level-2 data is sampled (see Section 4.1 for more details on Level-3U sampling). Level-3C products are also defined on Latitude-Longitude grid (here 0.5° resolution) onto which the properties are averaged or their frequency collected (histograms). Further separation of cloud properties in Level-3C in e.g. day/night, liquid/ice, were made wherever suitable (see

Table 1-4).

Table 1-2 List of generated cloud properties. CMA/CFC and CPH are derived in a pre-processing step. In the next step, COT, CER and CTP are retrieved simultaneously by fitting a physically consistent cloud/atmosphere/surface model to the satellite observations using optimal estimation (OE). Moreover, LWP and IWP are obtained from COT and CER. In addition, spectral cloud albedo (CLA) for two visible channels are derived. In a post-processing step, derived cloud properties and ERA-Interim information are used to determine radiative broadband fluxes. The Photosynthetically active radiation (PAR) is no standard output.

Variable	Abbrev.	Definition
Cloud mask / Cloud fraction	CMA/ CFC	A binary cloud mask per pixel (L2, L3U) and therefrom derived monthly total cloud fractional coverage (L3C) and separation into 3 vertical classes (high, mid-level, low clouds) following ISCCP classification (Rossow and Schiffer, 1999).

 cloud cci	Doc:	Cloud_cci_D2.1_ATBD_v6.2.doc			
	Date:	14 October 2019			
	Issue:	6	Revision:	2	Page 8

Variable	Abbrev.	Definition
Cloud phase	CPH	The thermodynamic phase of the retrieved cloud (binary: liquid or ice; in L2, L3U) and the therefrom derived monthly liquid cloud fraction (L3C).
Cloud optical thickness	COT	The line integral of the absorption coefficient and the scattering coefficient (at 0.55 μ m wavelength) along the vertical in cloudy pixels.
Cloud effective radius	CER	The area-weighted radius of the cloud drop and crystal particles, respectively.
Cloud top pressure/ height/ temperature	CTP/ CTH/ CTT	The air pressure [hPa] /height [m] /temperature [K] of the uppermost cloud layer that could be identified by the retrieval system.
Cloud liquid water path/ Ice water path	LWP/ IWP	The vertical integrated liquid/ice water content of existing cloud layers; derived from CER and COT. LWP and IWP together represent the cloud water path (CWP)
Joint cloud property histogram	JCH	This product is a spatially resolved two-dimensional histogram of combinations of COT and CTP for each spatial grid box.
Spectral cloud albedo	CLA	The blacksky cloud albedo derived for channel 1 (0.67 μ m) and 2 (0.87 μ m), respectively (experimental product)
Cloud effective emissivity	CEE	cloud radiative thickness in the infrared typically referred to as the “effective emissivity”
Top of atmosphere upwards/downwards flux	TOA	Shortwave (SW) and longwave (LW) fluxes at the Top of the atmosphere, upwelling and downwelling
Top of atmosphere upwards/downwards flux - clear-sky	TOA _{clear}	Shortwave (SW) and longwave (LW) fluxes at the Top of the atmosphere, upwelling and downwelling - for clear sky conditions
Bottom of atmosphere (surface) upwards/downwards flux	BOA	Shortwave (SW) and longwave (LW) fluxes at the Bottom of the atmosphere, upwelling and downwelling
Bottom of atmosphere (surface) upwards/downwards flux - clear-sky	BOA _{clear}	Shortwave (SW) and longwave (LW) fluxes at the Bottom of the atmosphere, upwelling and downwelling - for clear sky conditions
Photosynthetically active radiation	PAR	Bottom of atmosphere incoming shortwave radiation in the spectral range between 400 and 700nm



	Doc:	Cloud_cci_D2.1_ATBD_v6.2.doc			
	Date:	14 October 2019			
	Issue:	6	Revision:	2	Page 9

Table 1-3 Processing levels of Cloud_cci data products. Level-3U and Level-3C are each directly derived from Level-2.

Processing level	Spatial resolution	Description
Level-2 (L2)	AATSR: 1km AVHRR: 5 km	Retrieved cloud variables at satellite sensor pixel level, thus with the same resolution and location as the sensor measurements (Level-1)
Level-3U (L3U)	Latitude-Longitude grid at 0.05° res.	Cloud properties of Level-2 orbits projected onto a global space grid without combining any observations of overlapping orbits. Only subsampling is done. Common notation for this processing level is also L2b. Temporal coverage is 24 hours (0-23:59 UTC).
Level-3C (L3C)	Latitude-Longitude grid at 0.5° res.	Cloud properties of Level-2 orbits of one single sensor combined (averaged / sampled for histograms) on a global space grid. Temporal coverage of this product is 1 month.


Table 1-4 Cloud_cci product features incl. day and night separation, liquid water and ice as well as histogram representation. Level-3U refers to the un-averaged, pixel-based cloud retrievals sampled onto a global Latitude-Longitude (lat/lon) grid. ¹CMA in Level-2 and Level-3U is a binary cloud mask. All products listed exist in each dataset listed above.

	Level 2 swath based 1km/5km	Level-3U daily sampled global 0.05° lat/lon grid	Level-3C monthly averages global 0.5° lat/lon grid	Level-3C monthly histograms global 0.5° lat/lon grid
CMA/CFC	✓ as CMA ¹	✓ as CMA ¹	✓ day/night/high/mid/low	-
CTP, CTH, CTT	✓	✓	✓	✓ liquid/ice
CPH	✓	✓	✓ day/night	-
COT	✓	✓	✓ liquid/ice	✓ liquid/ice
CER	✓	✓	✓ liquid/ice	✓ liquid/ice
LWP	✓ as CWP	✓ as CWP	✓	✓ as CWP
IWP			✓	
CLA	✓ 0.6/0.8µm	✓ 0.6/0.8µm	✓ 0.6/0.8µm	✓ 0.6/0.8µm/liquid/ice
JCH	-	-	-	✓ liquid/ice
TOA_{up,dn,sw,lw}	✓	✓	✓	-
BOA_{up,dn,sw,lw}, PAR	✓	✓	✓	-

 cloud cci	Doc:		Cloud_cci_D2.1_ATBD_v6.2.doc		
	Date:		14 October 2019		
	Issue:	6	Revision:	2	Page 10

1.4 Uncertainties

The retrieved cloud properties CMA, CTP, CTT, CTH, COT, CER, LWP and IWP (for CC4CL also CLA) are accompanied by pixel-based (Level-2) uncertainties, which are output of the OE technique and represent a rigorous propagation of the uncertainties in the input data, e.g. a-priori information, measurements, radiative transfer. These uncertainties values represent the 68% confidence interval of the true value being within the retrieved value \pm uncertainty. These Level-2 uncertainties are also given in Level3U and further propagated into Level-3C. For this a sound mathematical framework has been developed and implemented taking into account the retrieval uncertainties but also the uncertainty correlations. The framework allows an estimation of both the real variability of the observed property and the uncertainty of the calculated mean. Determine and utilizing the uncertainty correlation is a particular key point for an appropriate propagation of Level-2 uncertainties into higher-level products (e.g. Level-3C). Please see the Comprehensive Error Characterization Report ([CECRv3](#)) and [Stengel et al. \(2017\)](#) for further details on the uncertainty measures provided. Results of uncertainty validation are given in PVIRv6.

	Doc:	Cloud_cci_D2.1_ATBD_v6.2.doc		
	Date:	14 October 2019		
	Issue:	6	Revision:	2
Page 11				

2. Satellite sensors and their measurement records

An important aspect for any product-based climate dataset (formally denoted Thematic Climate Data Records - TCDRs) is that retrieved products have been derived from accurately calibrated and homogenized radiances (formally denoted Fundamental Climate Data Records - FCDRs). In the ESA Cloud_cci Phase 1, studies were made to evaluate currently available Level 1 datasets. These studies concentrated on the first product demonstration period 2007-2009.

In the ESA Cloud_cci Phase 2, processing of a much longer time period were carried out: > 30 years for AVHRR, > 10 years for MODIS data and 10 years for AATSR and MERIS data. In the following sections we describe which Level 1 were used and how these datasets were prepared (if applicable).

2.1 AVHRR


Sensor characteristics

Measurements from the Advanced Very High Resolution Radiometer (AVHRR) radiometer on board the polar orbiting NOAA satellites and the EUMETSAT MetOp satellites have been performed since 1978. The instrument only measured in four spectral bands in the beginning (AVHRR/1), but from 1982 a fifth channel was added (AVHRR/2) and in 1998 even a sixth channel ($1.6 \mu\text{m}$) was made available (AVHRR/3), although only accessible if switched with the previous third channel at $3.7 \mu\text{m}$.

Table 2-1 describes the AVHRR instrument, its various versions and the satellites carrying them. The AVHRR instrument measures at a horizontal resolution close to 1 km at nadir but only data at a reduced resolution of approximately 4 km are permanently archived and available with global coverage since the beginning of measurements. This dataset is denoted Global Area Coverage (GAC) AVHRR data. See Figure 2-1 for a schematic description of the GAC generation.

Table 2-1 *Spectral channels of the Advanced Very High Resolution Radiometer (AVHRR). The three different versions of the instrument are described as well as the corresponding satellites. Notice that channel 3A was only used continuously on NOAA-17 and Metop-A. For the other satellites carrying AVHRR/3, channel 3A was used only for shorter periods.*

Channel Number	Wavelength (μm) AVHRR/1 NOAA-6,8,10	Wavelength (μm) AVHRR/2 NOAA-7,9,11,12,14	Wavelength (μm) AVHRR/3 NOAA-15,16,17,18 NOAA-19, Metop-A
1	0.58-0.68	0.58-0.68	0.58-0.68
2	0.725-1.10	0.725-1.10	0.725-1.10
3A	-	-	1.58-1.64
3B	3.55-3.93	3.55-3.93	3.55-3.93
4	10.50-11.50	10.50-11.50	10.50-11.50
5	Channel 4 repeated	11.5-12.5	11.5-12.5

	Doc:		Cloud_cci_D2.1_ATBD_v6.2.doc		
	Date:		14 October 2019		
	Issue:	6	Revision:	2	Page 12

AVHRR data record used in Cloud_cci

As a baseline for Cloud ECV production in Phase 2 the calibration work of NOAA ([Heidinger et al., 2010](#)) was used, which corrects the visible and 1.6 μm channels of AVHRR. The calibration was updated based on an improved calibration reference in MODIS Collection 6 (Heidinger, 2014, personal communication). This update was the basis for the production of an (intermediate) FCDR which was used in Cloud_cci for the production of the AVHRR-based ECV datasets. The calibration of infrared AVHRR channels is basically left untouched since on-board blackbody calibration targets were found to provide stable and reliable results. However, for future upgrades of the AVHRR FCDR remaining issues with the infrared channels (e.g., see [Mittaz and Harris \(2009\)](#)) need to be addressed.

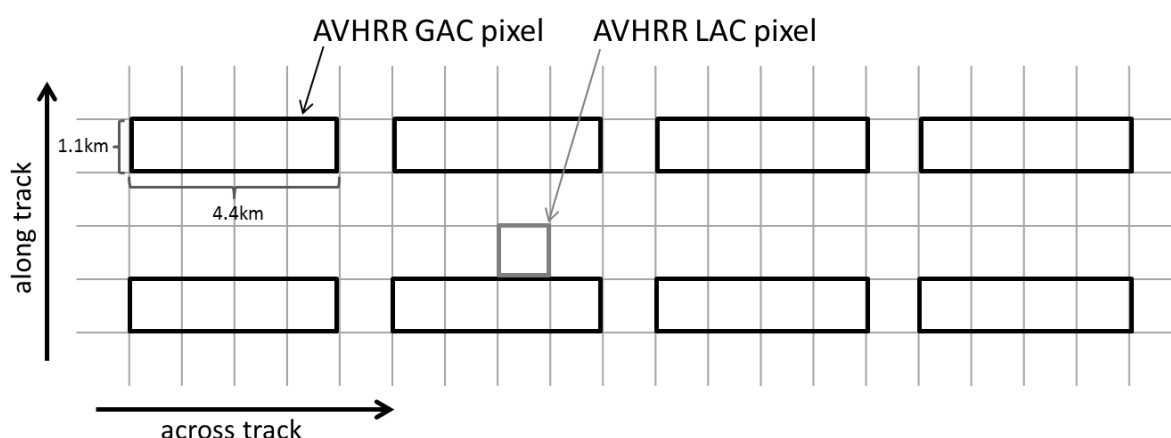


Figure 2-1 Schematic view on the conversion of original AVHRR 1 km pixel (Local area coverage - LAC) data to the GAC format.

The upgraded calibration and inter-calibration is realised through the use of a new pre-processing module, denoted PyGAC. PyGAC is an open-source community-driven Python interface to read and calibrate raw level 1b AVHRR GAC data. PyGAC takes advantage of the modular and object oriented philosophy of the Python programming language and its vast cache of public utilities.

For each AVHRR GAC orbit, PyGAC provides calibrated reflectances and brightness temperatures, sun and satellite zenith and azimuth angles and scanline quality information. The output files have HDF5 and netCDF formats and follow international Climate and Forecast conventions. In addition to calibration improvements, also the geolocation is improved for the historical part of AVHRR data (second generation, AVHRR/2) using clock-drift corrections provided by the University of Miami. The PyGAC interface is easily adaptable to be able to compute independent navigation information. A publication describing PyGAC in more details is under preparation. Most important aspects of this task are also documented in [RAFCDRv1.0](#).

For potential future application of the AVHRR Level-1 data, it is the ambition to take on board potential improvements resulting from the WMO Space Programme activity “Advancing the AVHRR FCDR) coordinated by the SCOPE-CM (Sustained, Coordinated Processing of Environmental Satellite Data for Climate Monitoring) programme. As a further complement to these calibration improvements, also navigation corrections will have to be improved for some of the early afternoon satellites utilising pre-existing information on clock errors.

2.2 AATSR

Sensor characteristics

AATSR has seven spectral bands in the solar, near-infrared and infrared range between 0.55 μm and 12 μm . It scans the Earth's surface with a conically scanning mirror directing radiation from two apertures onto the radiometer. This enables the instrument to view the Earth at two different angles, the nadir view and the forward view at an angle of 55° from the nadir. At nadir the pixel resolution is approximately $1 \times 1 \text{ km}^2$ with a swath width of 512 pixels. The instrument is designed to be self-calibrating, with two integrated thermally controlled black-body targets for calibration of the thermal channels as well as an opal visible calibration target, which is illuminated by sunlight, for the visible/near-infrared channels. Central wavelengths and bandwidths of each AATSR channel are given in Table 2-3.

Table 2-2 AATSR spectral channels

Channel	Wavelength [nm]	Bandwidth [nm]
1	550	20
2*	665	20
3*	865	20
4	1610	60
5*	3740	380
6*	10850	900
7*	12000	1000


* AVHRR-heritage channels of AATSR used in CC4CL

ATSR-2/AATSR data record used in Cloud cci

The ATSRs are designed to have exceptional long term sensitivity and stability of calibration. Thermal channels are calibrated using two on board black bodies at known temperatures which are observed during each across-track scan of the instrument. This makes it possible to determine single channel equivalent brightness temperatures correct to 0.05K (Smith et al., 2001). The instrument also has an on board visible/near-infrared calibration system enabling the visible channels to be calibrated to an accuracy of better than 4% (Smith et al., 2008), which is subsequently improved via vicarious calibration using scenes of known stable surface BRDF (certain deserts and ice caps).

The vicarious calibration must be applied to the ATSR and AATSR level1b visible channel data before level2 data processing can begin. The vicarious calibration correction is updated regularly and can be accessed at <http://www.aatsrops.rl.ac.uk/EDSX/OtherInfo/>.

Complementary to the vicarious calibration based on surface reference sites, inter-comparisons between Aqua-MODIS and AATSR radiances (with previous vicarious calibration corrections applied) were performed using the SNO approach. Because of the orbit differences of ENVISAT and Aqua, SNOs were only possible at latitudes close to 70°N and 70°S . Figure 2-2 below shows results for the AATSR AVHRR-heritage channels at 665 nm, 865 nm and 1610 nm. Note that results are based exclusively on SNO targets matching the criteria of being well-illuminated (i.e., having solar zenith angles below 70°), not too dark (i.e., reflectance factors above 10 %) and homogeneous (i.e., internal reflectance standard deviation less than 1 %). Table 2-3 summarises SNO results for all channels (including also infrared channels at 3.7, 10.8 and 12.0 microns).

	Doc:	Cloud_cci_D2.1_ATBD_v6.2.doc		
	Date:	14 October 2019		
	Issue:	6	Revision:	2
		Page 14		

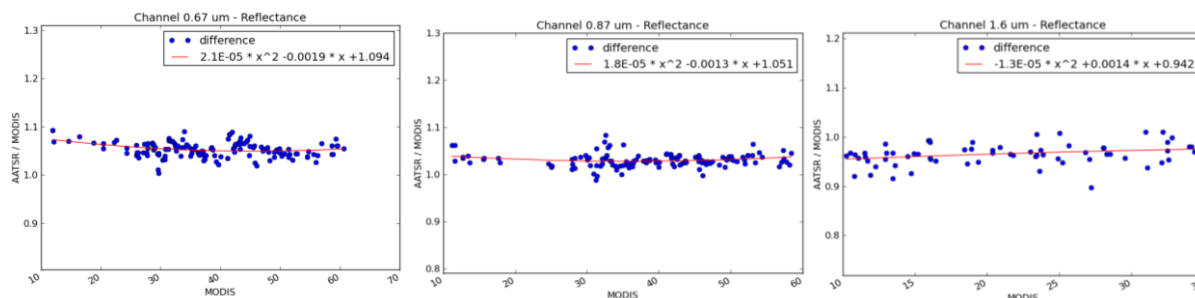


Figure 2-2 AATSR reflectance factor quotas with respect to MODIS at 0.67 micron (a), 0.87 micron (b), 1.6 micron (c) for SNO targets collected in the period 2007-2009. Results are from Karlsson and Johansson (2014).

Table 2-3 Reflectance factor quota (AATSR/MODIS) or brightness temperature quota with respect to MODIS-Aqua deduced from SNO inter-comparisons in the period 2007-2009. Results are from Karlsson and Johansson (2014).

AATSR channel	Wavelength [nm]	Reflectance factor quota or Brightness temperature quota
1	550	n.a.
2	665	1.050
3	865	1.029
4	1610	0.965
5	3740	1.000
6	10850	1.000
7	12000	0.999

Results show higher AATSR reflectances (5.0 % and 2.9 %, respectively) for channels 2 and 3 but about 3.5 % lower reflectances in channel 4 than MODIS. No trend was indicated for channels 2 and 3 but a slightly increasing AATSR trend (i.e., decreasing difference compared to MODIS) was noticed for channel 4. For infrared channels, the agreement appears to be very good.

Deviations for two of the visible channels can be compared to Figure 2-3 showing corresponding results over surface reference sites as presented by Bouvet et al. (2012). Here, measured reflectances have been compared to modelled radiances for the surface sites collected during approximately the same time period (2006-2009). We notice a relative difference between AATSR and MODIS reflectances of approximately 3 % at 660 nm and 4 % at 870 nm. This agrees reasonably well with results presented in Table 2-3.

The nature of the differences found for the visible channels still remains to be not fully understood. However, studies of the influence of various spectral variations of the surface site reflectance and the atmosphere (transferred via different spectral response functions - elaborated in further detail in Bouvet et al., 2012) indicate that this can explain most of the difference. Thus, inter-comparison methods must be able to compensate better for these effects before firm conclusions about any remaining calibration biases can be made and further applied in calibration correction methods. Consequently, it was decided to stay with the current AATSR calibration based on vicarious calibration from surface sites for cloud products generated for the period 2007-2009.

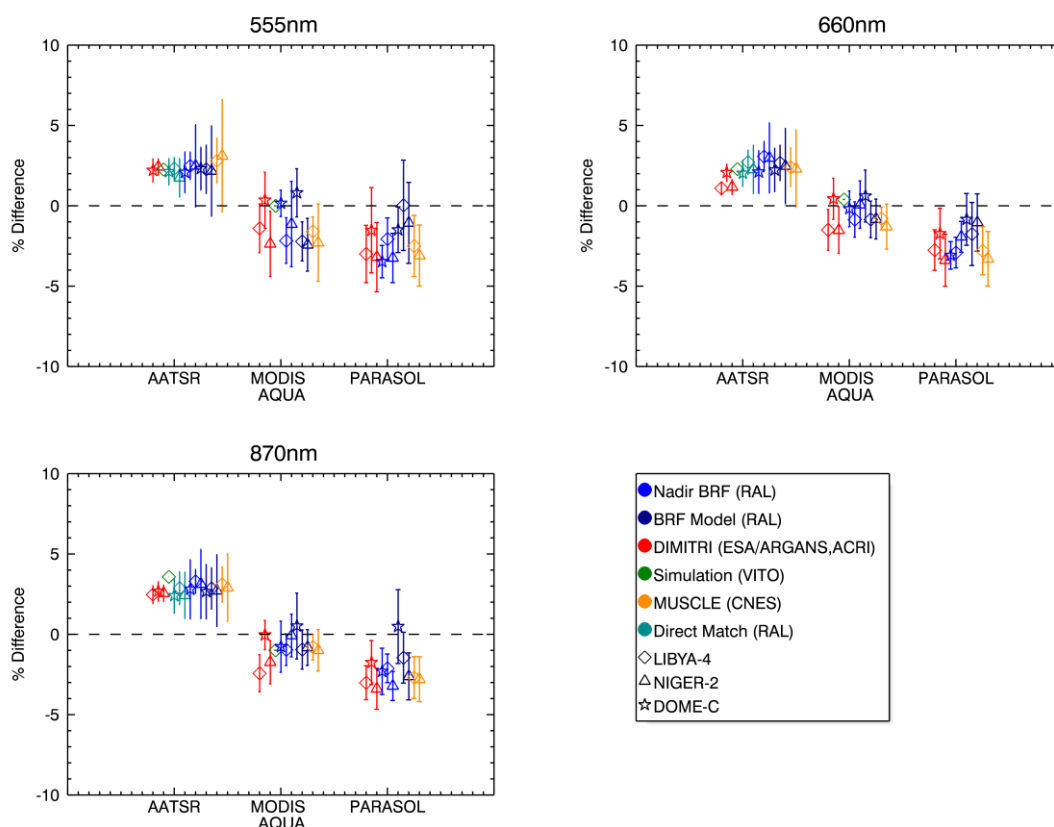



Figure 2-3 Intercomparisons using direct matchups, nadir BRF and full BRF model including a correction for systematic uncertainties. Error bars represent the $k=1$ standard deviation of the differences between the measurements and reference (from Bouvet *et al.*, 2012).

2.3 Limitations of the (inter-)calibration

Inter-comparisons with MODIS-Aqua data concerning the three sensors AVHRR, AATSR and MERIS have shown good agreement for AVHRR and MERIS (i.e., deviation limited to 1-2 % for visible reflectances and as low as 0.1 % for infrared radiances). Larger deviations (up to 5 %) have been seen for AATSR. Because of limitations in the number of available inter-calibration targets (e.g., based on the SNO approach) as a consequence of the short period (three years) plus additional remaining uncertainties regarding effects for spectral differences (especially for AATSR), it has not been possible to firmly establish specific calibration corrections as an addition or complement to existing vicarious calibration corrections. For this reason and to evaluate potential trends, a longer evaluation period and access to improved spectral correction methods appear necessary.

	Doc:		Cloud_cci_D2.1_ATBD_v6.2.doc		
	Date:		14 October 2019		
	Issue:	6	Revision:	2	Page 16

3. The Community Cloud retrieval for CLimate (CC4CL) retrieval system

CC4CL consists of three main components: cloud detection, cloud typing and OE-based cloud property retrieval, which are summarized in the following subsections. As a post-processing step radiative broadband flux properties are derived.

3.1 Cloud detection

The cloud detection is based on artificial neural networks (ANNs) that have been trained using AVHRR-NOAA-18 measurements and collocated CALIOP cloud optical depth (COD) for a subset of all available CALIOP-AVHRR-NOAA18/19 collocation in 2007 to 2014. The applied ANN outputs mimicked CALIOP COD (ANNCOD) in the range of 0 to 1. To convert the ANNCOD to a needed binary cloud decision, thresholds are applied which depend on illumination conditions (day/night/twilight) and region (land/sea). Verification scores were calculated, using the training data set, based on the ANNCOD output and the threshold applied, which are used to determine the uncertainty of the cloud mask decision per pixel.

Compared to [ATBDv5.0](#) and [ATBD-CC4CLv5.0](#) the presented cloud detection was retrained using a much larger training dataset: one full year of collocations with CALIOP instead of data of 12 days. In addition the NIR channel (1.6 μ m or 3.7 μ m depending on sensor) were introduced, which improved cloud detection over snow and ice surfaces considerably. More information about the cloud detection can be found in [ATBD-CC4CLv6.1](#) and [Stengel et al. \(2019\)](#).

3.2 Cloud typing & phase

Typing


Cloud typing is based on developments by Pavolonis and Heidinger (2004) and Pavolonis et al. (2005), which is based on a threshold decision tree. Cloud type output classes are:

- clear
- switched to water* (liquid)
- fog (liquid)
- water (liquid)
- supercooled (liquid)
- switched to ice* (ice)
- opaque ice (ice)
- cirrus (ice)
- deep convective (ice)
- overlap (ice)

The classes switched-to-water and switched-to-ice are additional classes introduced by Cloud_cci which account for too warm ice clouds (according to CTT) being reclassified to water and too cold liquid clouds being reclassified as ice.

Phase

In contrast to dataset versions 2, for which the cloud types (see above) were converted to a binary cloud phase information (see [ATBDv5.0](#) and [ATBD-CC4CLv5.0](#)), an artificial neural network was trained and applied for the phase determination in v3 datasets. Similar to the cloud detection, the ANN for cloud phase received input by collocating AVHRR measurements with CALIOP cloud phase information. The output of the ANN ranges from 0 to 1, imposing the need for applying a threshold to the output to infer a binary phase information. Exact input setting and the threshold used are reported in [Stengel et al. \(2019\)](#). More information about the cloud typing can be found in [ATBD-CC4CLv6.0](#).

	Doc:		Cloud_cci_D2.1_ATBD_v6.2.doc		
	Date:		14 October 2019		
	Issue:	6	Revision:	2	Page 17

3.3 Optimal estimation retrieval of cloud properties

The CC4CL retrieval of cloud properties is based on ORAC (Optimal Retrieval of Aerosol and Cloud) algorithm (Poulsen et al., 2012 and Watts et al., 1998, but including further developments made in the Cloud_cci Project: Sus et al. (2017), McGarragh (2017) and ATBD-CC4CLv6.1). The retrieval is based on the optimal estimation technique and can be used to determine both aerosol and cloud properties from visible/infrared satellite radiometers. In the case of cloud retrievals the algorithm, models the surface properties, atmosphere and subsequent fits the cloud properties using LUTs created from DIScrete Ordinates Radiative Transfer (DISORT) (Stamnes et al. 1998) to the TOA signal measured by the satellite by varying the cloud optical depth, effective radius, cloud top pressure, phase and surface temperature. From these retrieved products we can subsequently derive liquid and ice water path. The optimal estimation framework of CC4CL provides some key advantages such as

- Comprehensive propagation of the measurement and forward model error into the final product.
- The ability to include prior knowledge of the retrieved quantities together with the uncertainties in a priori knowledge.
- A mathematically rigorous estimate of the uncertainty on retrieved values on a pixel by pixel basis by propagating the uncertainties of the measurements, model and a priori data.
- The retrieval also provides an indicator ('the cost') of the appropriateness of the model used.

A specific advantage of this algorithm is that it uses all channels and derives all parameters simultaneously. Hence the algorithm provides a measure of the consistency between retrieval representation of cloud and satellite radiance. The current version of CC4CL uses ORAC with RTTOV to calculate the clear sky radiances in the visible and infrared. The derived pixel level cloud properties are listed in Table 1-2, of which CTP, COT, CER are part of the state vector in the optimal estimation, while all others are derived. A summary is given in Table 3-1. More detailed information on the ORAC system can be found in McGarragh (2017) and ATBD-CC4CLv6.1, with the latter also holding information about recent developments.¹.


3.4 Calculation of the broadband fluxes

Broadband radiative fluxes are computed in a post-processing step of the CC4CL using BUGSrad (Stephens et al., 2001). BUGSrad is based on the two-stream approximation and correlated-k distribution methods of atmospheric radiative transfer. The basis of the algorithm is the same as that described by Fu and Liou (1992). It is applied to a single-column atmosphere for which the cloud and aerosol layers are assumed to be plane-parallel. Cloud properties retrieved using CC4CL are ingested into BUGSrad to compute both shortwave and longwave radiative fluxes for the top and bottom of atmosphere. The algorithm uses 18 bands that span the entire electromagnetic spectrum to compute the broadband flux. In total, 6 bands are used for shortwave and 12 bands are used for longwave radiative flux calculations. In depth information about BUGSrad and its application can be found in ATBD-CC4CL-TOA_FLUXv1.0. Comparisons to surface and other satellite data are presented in Stengel et al. (2019).

3.5 Limitations

A full list of the assumptions and uncertainties are outlined in the uncertainty characterisation document (CECRv4). The main assumptions are listed below.

1. The CC4CL cloud algorithm as implemented within the Cloud_cci uses only the heritage channels.

	Doc:		Cloud_cci_D2.1_ATBD_v6.2.doc		
	Date:		14 October 2019		
	Issue:	6	Revision:	2	Page 18

2. The CC4CL cloud model assumes a single layer of cloud. No a priori climatological information is used in the retrieval to constrain the cloud heights hence the cloud height retrieved is the radiative effective cloud height in the case of multi-layer clouds.
3. The CC4CL cloud retrieval uses the IR channels to assign the cloud height. The penetration depth of the IR clouds is approximately 1 optical depth into the cloud layer. The cloud height assignment and associated phase will be influenced by this, typically leading to a overestimation of the derived cloud top pressure (underestimation of cloud top height). An attempt to account for the semitransparency of many uppermost cloud layers is documented in Section 2.3.10 of [ATBD-CC4CLv6.1](#).
4. The effective radius and optical depth retrievals are strongly dependent on the choice of optical properties used. The effective radius will differ for the 1.6 and 3.7 μ m retrievals if the vertical profile of effective radius changes with height. The 1.6 μ m channel penetrates deeper into the cloud.



	Doc:	Cloud_cci_D2.1_ATBD_v6.2.doc			
	Date:	14 October 2019			
	Issue:	6	Revision:	2	Page 19

Table 3-1 CC4CL in a nutshell.

	CC4CL
History	ORAC which was originally developed for application to SEVIRI (OCA, P. Watts). Applied to ATSR under nationally funded project GRAPE by RAL and University of Oxford. Further developed in ESA Cloud_cci to be applicable to AVHRR, MODIS, AATSR and successor sensors.
COT	1. All cloud parameters retrieved simultaneously. NWP profiles calculated using RTTOV 2. Post correction of CTP/CTH for boundary layer inversion situations 3. Vis/NIR LUTS derived using DISORT RTM
CER	
CTP	
LWP	$LWP = 4/3 (\tau \cdot re \cdot pwat / Qwat)$; $Qwat = 2$ (τ : optical thickness, re : effective radius, $pwat$: density liquid water)
IWP	$IWP = 4/3 (\tau \cdot re \cdot pice / Qice)$; $Qice = 2.1$ (τ : optical thickness, re : effective radius, $pice$: density ice water)
Ice	Baum Ice crystals
Phase Discrimination	Cloud typing is based on Pavolonis et al. (2005), cloud phase is based on ANN with posterior application of scene dependent thresholds to derived a binary phase information.
Cloud Mask	An ANN based retrieval is applied to all pixels including a posterior application of scene dependent threshold to the ANN output of a pseudo CALIPSO COD yielding into a binary cloud mask information.
Broadband fluxes	Using the retrieved properties CER, COT, CTP and Stemp in addition to thermodynamic profiles from reanalysis data, broadband fluxes are calculated at TOA and BOA (upwelling+downwelling, shortwave+longwave) at each satellite pixel.
Snow/Ice discrimination	Snow and sea ice information is used from the NSIDC data base. Alternatively, ERA-Interim snow and ice information can be chosen. The information is used to modify the surface albedo.
Errors Quality Control	Cost function provides an indication of the quality of the fit to the cloud model. If the fit is good then the errors indicate the accuracy of the retrieval. Convergence test: ORAC uses the change in the cost function between iterations to determine whether a retrieval is said to have converged. Errors considered <ol style="list-style-type: none"> 1. Measurement errors 2. Cloud inhomogeneity 3. Coregistraion error 4. Surface contribution
Comments	Single layer plane parallel cloud assumed for all instruments. State vector also contains surface temperature.

	Doc:	Cloud_cci_D2.1_ATBD_v6.2.doc			
	Date:	14 October 2019			
	Issue:	6	Revision:	2	Page 20

4. Generation of the Level-3 products

The Cloud_cci data products are available at different processing levels including sensor-specific pixel level products (Level-2), sensor-specific global composites (Level-3U) and sensor specific averaged products on a global grid (Level-3C). Details on the processing levels are reported in Table 1-3. All available Level-2 data are input to the Level-3 processing software.

The Level-3U/-3C grid is an equal angle grid covering the full globe. For the L3U sampled product the horizontal resolution is 0.05 degrees, while for Level-3C the spatial resolution is 0.5 degrees. The actual gridding is a straightforward process in which the latitude and longitude information of each L2 pixel is used to determine the indices of the corresponding grid cell the pixel falls into. This depends on the desired grid resolution.

The subsections below outline the averaging techniques applied for generation of the Level-3C data.

4.1 Level-3U products

In order to reduce the amount of data and to map the data to a regular grid but without losing all the horizontal variability by averaging it, a sampling technique has been implemented which is based on choosing the minimum satellite viewing zenith angle. This means that in the final product the pixel with the smallest satellite viewing zenith angle of all pixels falling into the grid cell is chosen to represent that grid cell. This is motivated by the fact that such a pixel is located closest to satellite nadir, which means that undesired effects due to a slant viewing path across the atmosphere are minimal. Since the footprint size increases with increasing satellite viewing angle, the grid cell that are covered by the footprint are calculated individually for each satellite pixel. This leads to that more than one grid cell can be filled with one individual observation depending on footprint size. Additionally, the L3U product is split up in ascending and descending satellite nodes. The viewing zenith angle sampling and the separation into the two nodes effectively leads to a larger temporal and spatial coherence of atmospheric patterns.

4.2 Level-3C products

4.2.1 Aggregating cloud mask and phase information


Cloud mask information consists of three stages: no information available (Fill value), clear (0) and cloudy (1). Averages are produced by counting the instances of clear and cloudy cloud mask information for each grid cell and evaluation of:

$$CC(i, j) = \frac{N(i, j)_{Cloudy}}{N(i, j)_{Cloudy} + N(i, j)_{Clear}}$$

4.2.2 Aggregating microphysical and macrophysical cloud properties

To ensure consistency when averaging the cloud properties, only those pixels are considered for which all cloud variables are available. However, not for all cloudy pixels the cloud retrieval yields valid results, thus the pixels used for averaging cloud properties is usually a subset of those being identified as cloud (and used in the cloud fraction estimation). During night-time apparently no consistence between micro and microphysical properties can be achieved due to the absence of microphysical retrievals.

The unweighted mean and standard deviation for grid cell (i, j) are then defined as:

	Doc:	Cloud_cci_D2.1_ATBD_v6.2.doc			
	Date:	14 October 2019			
	Issue:	6	Revision:	2	Page 21

$$\langle x(i, j) \rangle = \frac{1}{N(i, j)_{Cloudy}} \sum_{k=1}^{N(i, j)_{Cloudy}} x_k(i, j)$$

$$s(x(i, j)) = (\langle x^2(i, j) \rangle - \langle x(i, j) \rangle^2)^{0.5}$$

Where i and j are the longitude and latitude indices. The error weighted mean and standard deviation for grid cell (i, j) are defined as:

$$\langle x(i, j) \rangle_w = \frac{1}{W_1} \sum_{k=1}^{N(i, j)_{Cloudy}} x_k(i, j) w_k(i, j)$$

$$s(x(i, j))_w = \left(\frac{W_1}{W_1^2 - W_2} \langle x^2(i, j) \rangle_w - \langle x(i, j) \rangle_w^2 \right)^{0.5}$$

With:

$$W_1 = \sum_{k=1}^{N(i, j)_{Cloudy}} w_k; W_2 = \sum_{k=1}^{N(i, j)_{Cloudy}} w_k^2; w_k = \frac{1}{\sigma_k}$$

σ_k is the retrieval error of the corresponding variable. This approach is pursued for all micro- and macrophysical variables except for the cloud phase, for which, similar to the cloud cover, the number of liquid cloud instances per grid box is counted and

$$\langle cty(i, j) \rangle = \frac{N(i, j)_{Cloudy}^{Liquid}}{N(i, j)_{Cloudy}}$$

is computed to give the liquid cloud phase contribution for grid box (i, j) . Similar, the liquid and ice water paths are computed as:

$$\langle lwp(i, j) \rangle = \frac{1}{N(i, j)_{Cloudy}^{Liquid}} \sum_{k=1}^{N(i, j)_{Cloudy}^{Liquid}} cwp_{liquid}$$

$$\langle iwp(i, j) \rangle = \frac{1}{N(i, j)_{Cloudy}^{Ice}} \sum_{k=1}^{N(i, j)_{Cloudy}^{Ice}} cwp_{Ice}$$


Here, cwp_{Liquid} and cwp_{Ice} are distinguished by the cloud phase flag which is also used in counting the liquid and ice instances for $N(i, j)_{Cloudy}^{Liquid}$ and $N(i, j)_{Cloudy}^{Ice}$. These quantities are therefore connected by:

$$\langle cwp(i, j) \rangle = \langle cty(i, j) \rangle \langle lwp(i, j) \rangle + (1 - \langle cty(i, j) \rangle) \langle iwp(i, j) \rangle$$

Furthermore, to account for the special structure of the cloud top pressure for this variable the logarithmic average is computed additionally:

$$\langle ctp(i, j) \rangle_{\ln} = \exp\left(\frac{1}{N(i, j)_{Cloudy}} \sum_{k=1}^{N(i, j)_{Cloudy}} \ln(ctp_k(i, j))\right)$$

Apart from those products referring to grid cell averages, 2D ISCCP-like histograms are also produced for each cell which partitions the CTP and COT space.

	Doc:	Cloud_cci_D2.1_ATBD_v6.2.doc			
	Date:	14 October 2019			
	Issue:	6	Revision:	2	Page 22

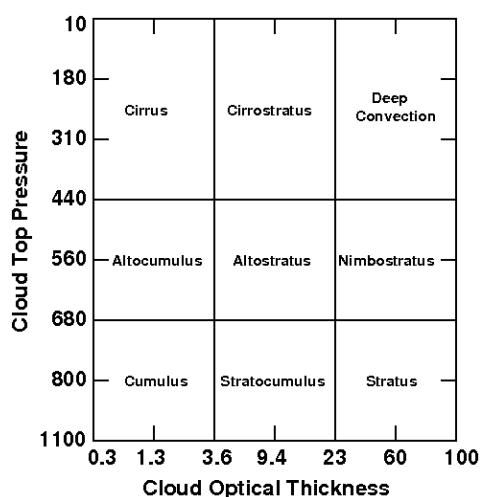


Figure 4-1 ISCCP-like 2D cloud top pressure vs. cloud optical thickness histogram.

The widths of the bins are defined as follows:

- COT: {0, 0.3, 0.6, 1.3, 2.2, 3.6, 5.8, 9.4, 15, 23, 41, 60, 80, 100}
- CTP: {1, 90, 180, 245, 310, 375, 440, 500, 560, 620, 680, 740, 800, 875, 950, 1100} [hPa]


As can be seen in Figure 4-1, this partitioning is also associated with nine different cloud types and thus allows for cloud classification of the grid cell.

In addition to the 2D histogram, also 1D histograms are generated for the parameters CTP, CTT, CWP, COT, CER. Each histogram covers the solution space of its variable with the cloud phase as additional dimension. These histograms are provided on the spatial resolution of the level3 averages. The used bins are:

- CWP: {0, 5, 10, 20, 35, 50, 75, 100, 150, 200, 300, 500, 1000, 2000, inf} [g/m²]
- COT: {0.0, 0.3, 0.6, 1.3, 2.2, 3.6, 5.8, 9.4, 15.0, 23.0, 41.0, 60.0, 80.0, 100}
- CER: {0, 3, 6, 9, 12, 15, 20, 25, 30, 40, 60, 80} [μm]
- CTP: {1, 90, 180, 245, 310, 375, 440, 500, 560, 620, 680, 740, 800, 875, 950, 1100} [hPa]
- CTT: {200, 210, 220, 230, 235, 240, 245, 250, 255, 260, 265, 270, 280, 290, 300, 310, 350} [K].

4.2.3 Aggregation of broadband fluxes

The aggregation of the broadband fluxes are done in a similar fashion as the aggregation of the cloud properties (see Section 4.2.2), with the exception, that the fluxes are diurnal cycle corrected

	Doc:		Cloud_cci_D2.1_ATBD_v6.2.doc		
	Date:		14 October 2019		
	Issue:	6	Revision:	2	Page 23

to represent 24 hour means. This is in particular necessary for shortwave fluxes which heavily depend on the illumination conditions at the time of observation.

Longwave fluxes:

The diurnal cycle of LW fluxes was determined by applying CC4CL to two full days of SEVIRI observations. The mean diurnal cycle, as a function of surface type (land/sea), is then used to determine correction factors, depending on time of the day (thus on the time of observation), which are applied to each individual pixel observation to emulate a 24-hour mean, before averaging.

Shortwave fluxes:

Each shortwave flux observation is related to a specific solar zenith angle impacting the path length through the atmosphere as well as the angle under which the energy is reaching the Earth's surface. Using this information an individual diurnal cycle can be emulated for each pixel by sampling the varying solar zenith angle throughout 24 hours at the pixel location. The rescaled incoming and reflected solar radiation values from all of these samples are averaged to emulate a 24-hour mean for that pixel. This mean is then used to determine monthly means including all observations taken at that location throughout the month.

4.2.4 Limitations in the aggregation of Level-3 products


Level 3 generation

As already stated in the text above, all Level-2 data of the month are regarded as equally valid and are summed up to derive the monthly means. Under certain circumstances this could lead to the monthly mean being biased towards days for which more Level-2 data are available compared to others. The applied approach is thus in contrast to weighting each day equally within a month, which on the other hand might lead to few, spatiotemporally isolated observations being weighted too much. Under normal circumstances, under which the data coverage is nearly complete and nearly equally distributed within a month, the results of both approaches do not differ significantly.

Diurnal sampling

The diurnal cycle of clouds is well documented as a source of natural variability in the cloud field. It varies based on cloud type, latitude, season, and location. This cycle has significant effects on the horizontal and vertical distribution of clouds as well as on the cloud microphysical properties. The incomplete sampling of the diurnal cycle by polar orbiting satellite instruments, where usually 2 observations per day are taken for a specific place on Earth, introduces (1) differences between cloud data records of individual instruments when overpassing at significantly different local time, and (2) generally bias the cloud records compared to climatological means, for which more or less continuous observations within a day are required. By combining the records of the different sensors reduces the sampling error.

For proper interpretation of the temporal variability of individual Cloud_cci data records and among different records its diurnal cycle of cloud cover and possible methods to correct for it were assessed (RODCv1.0). However, Cloud_cci did not attempt to correct the cloud data records for the impact of the diurnal cycle, but rather provide the information. Corrections based on statistical analyses are inherently nonphysical and introduce uncertainty with little potential for information gain, however, they increase the stability of the time series.

	Doc:		Cloud_cci_D2.1_ATBD_v6.2.doc		
	Date:		14 October 2019		
	Issue:	6	Revision:	2	Page 24

5. References

ATBD-FAME-Cv5, Algorithm Theoretical Baseline Document (ATBD) FAME-C - ESA Cloud_cci, Issue 5, Revision: 0, planned date of Issue: 12/09/2017, Available at: <http://www.esa-cloud-cci.org/?q=documentation>

ATBD-CC4CLv6.1, Algorithm Theoretical Baseline Document (ATBD) CC4CL - ESA Cloud_cci, Issue 6, Revision: 1, planned date of Issue: 24/12/2018, Available at: <http://www.esa-cloud-cci.org/?q=documentation>

ATBD-CC4CL_TOA_FLUXv1.1, Algorithm Theoretical Basis Document (ATBD) of the Community Code for CLimate (CC4CL) Broadband Radiative Flux Retrieval (CC4CL-TOAFLUX) - ESA Cloud_cci, Issue 1, Revision: 0, planned date of Issue: 01/03/2016, Available at: <http://www.esa-cloud-cci.org/?q=documentation>

Bodas-Salcedo, A., Webb, M.J., Bony, S., Chepfer, H., Dufresne, J.L., Klein, S.A., Zhang, Y., Marchand, R., Haynes, J.M., Pincus, R. and John, V.O., **2011**. COSP: Satellite simulation software for model assessment. Bulletin of the American Meteorological Society, 92(8), p.1023.

Bouvet M., Adriaensen S., Barker K., Bourg L., Fougne B., Govaerts Y., Henry P., Kent C., Smith D. and Sterckx S., "CEOS IVOS Working Group 4: Intercomparison of vicarious calibration methodologies and radiometric comparison methodologies over pseudo-invariant calibration sites", Report to CEOS IVOS, **2012**.

Carbajal Henken, C.K., Lindstrot, R., Preusker, R. and Fischer, J.: FAME-C: cloud property retrieval using synergistic AATSR and MERIS observations. Atmos. Meas. Tech., 7, 3873-3890, doi:10.5194/amt-7-3873-2014, **2014**

CECRv4, Comprehensive Error Characterization Report (CECR) - ESA Cloud_cci, Issue 4, Revision: 1, Date of Issue: 06/05/2018, Available at: <http://www.esa-cloud-cci.org/?q=documentation>

Donlon, C., B. Berruti, A. Buongiorno, M.-H. Ferreira, P. Femenias, J. Frerick, P. Goryl, U. Klein, H. Laur, C. Mavrocordator, J. Nieke, H. Rebhan, B. Seitz, J. Stroede, R. Sciarra, **2012**: The Global Monitoring for Environment and Security (GMES) Sentinel-3 mission. Remote Sens. of Environ., 120, 37-57

Eliasson, S., Karlsson, K. G., van Meijgaard, E., Meirink, J. F., Stengel, M., and Willén, U.: The Cloud_cci simulator for the ESA Cloud_cci climate data record and its application to a global and a regional climate model, Geosci. Model Dev. Discuss., <https://doi.org/10.5194/gmd-2018-212>, in review, **2019**.

Fell, F., and J. **Fischer**, **2001**: Numerical simulation of the light field in the atmosphere-ocean system using the matrix-operator method. J. Quant. Spectrosc. Radiat. Transfer, 3, 351-388.


Fu, Q. and **Liou, K. N.** (1992). On the correlated k-distribution method for radiative transfer in nonhomogeneous atmospheres. J. Atmos. Sci., 49:2153-2170.

Feofilov, A. G., C. J. Stubenrauch, S. Protopapadaki, and R. Armante, **2017**: Diurnal variation of high-level clouds from a synergy of the space-borne infrared sounders AIRS and IASI: detection and radiative effects. In preparation for submission to ACPD.

Fischer, J., and H. **Grassl**, **1984**: Radiative transfer in an atmosphere-ocean system: An azimuthally dependent matrix-operator approach. Appl. Opt., 23, 1035-1039.

Gomez-Chova, L., Camps-Valls, G., Calpe, J., Munoz, J., and J. Moreno: MERIS/AATSR Synergy Algorithms for cloud screening, aerosol retrieval and atmospheric correction: Cloud Screening ATBD. University of Valencia, SYN-UV-ATBD 1.0, January **2009**

Heidinger, A.K., W.C. Straka, C.C. Molling, J.T. Sullivan and X.Q. Wu, **2010**: Deriving an inter-sensor consistent calibration for the AVHRR solar reflectance data record. Int. J. Rem. Sens., 31(24), 6493-6517.

	Doc:	Cloud_cci_D2.1_ATBD_v6.2.doc			
	Date:	14 October 2019			
	Issue:	6	Revision:	2	Page 25

Heymsfield, A.J., Matrosov, S. and Baum, B., 2003. Ice water path-optical depth relationships for cirrus and deep stratiform ice cloud layers. *Journal of Applied Meteorology*, 42(10), pp.1369-1390.

Hollmann, R., Merchant, C.J., Saunders, R., Downy, C., Buchwitz, M., Cazenave, A., Chuvieco, E., Defourny, P., de Leeuw, G., Forsberg, R. and Holzer-Popp, T., 2013. The ESA climate change initiative: Satellite data records for essential climate variables. *Bulletin of the American Meteorological Society*, 94(10), pp.1541-1552.

Hollstein, A., Fischer, J., Carbajal 5 Henken, C., and Preusker, R.: Bayesian cloud detection for MERIS, AATSR, and their combination, *Atmospheric Measurement Techniques*, 8, 1757-1771, doi:10.5194/amt-8-1757-2015, <http://www.atmos-meas-tech.net/8/1757/2015/>, 2015.

Karlsson, K.-G.; Johansson, E. Multi-Sensor Calibration Studies of AVHRR-Heritage Channel Radiances Using the Simultaneous Nadir Observation Approach. *Remote Sens.* 2014, 6, 1845-1862.

Lindstrot, R., Preusker, R. and Fischer, J., 2010: The empirical correction of stray light in the MERIS oxygen A band channel, *J. Atmos. Oceanic Technol.*, 27 (7), 1185-1194.

McGarraugh, G. R., Poulsen, C. A., Thomas, G. E., Povey, A. C., Sus, O., Stapelberg, S., Schlundt, C., Proud, S., Christensen, M. W., Stengel, M., Hollmann, R., and Grainger, R. G.: The Community Cloud retrieval for CLimate (CC4CL) - Part 2: The optimal estimation approach, *Atmos. Meas. Tech.*, 11, 3397-3431, <https://doi.org/10.5194/amt-11-3397-2018>, 2018.

Mittaz, P.D. and R. Harris, 2009: A Physical Method for the Calibration of the AVHRR/3 Thermal IR Channels 1: The Prelaunch Calibration Data. *J. Atmos. Ocean. Tech.*, 26, 996-1019, doi: 10.1175/2008JTECHO636.1

Pavolonis, M. J. and Heidinger, A. K.: Daytime cloud overlap detection from AVHRR and VIIRS, *Journal of Applied Meteorology*, 43, 762-778, 2004.

Pavolonis, M. J., Heidinger A. K., and Uttal, T., Daytime Global Cloud Typing from AVHRR and VIIRS: Algorithm Description, Validation, and Comparisons, *J. Appl. Meteor.*, 44, 804-826, doi:10.1175/JAM2236.1, 2005.

Poulsen, C.A., Siddans, R., Thomas, G.E., Sayer, A.M., Grainger, R.G., Campmany, E., Dean, S.M., Arnold, C. and Watts, P.D., 2012. Cloud retrievals from satellite data using optimal estimation: evaluation and application to ATSR. *Atmospheric Measurement Techniques*, 5(8), pp.1889-1910.

Preusker, R., and R. Lindstrot, 2009: Remote sensing of cloud-top pressure using moderately resolved measurements within the oxygen A band—A sensitivity study. *J. Appl. Meteor. Climatol.*, 48, 1562-1574.

PUGv3.1, Product User Guide (PUG) - ESA Cloud_cci, Issue 3, Revision: 1, Date of Issue: 18/04/2017, Available at: <http://www.esa-cloud-cci.org/?q=documentation>

PVIRv4.1, Product Validation and Intercomparison Report (PVIR) - ESA Cloud_cci, Issue 4, Revision: 1, Date of Issue: 18/04/2017, Available at: <http://www.esa-cloud-cci.org/?q=documentation>


RAFCDRv1.0, Technical Report on AVHRR GAC FCDR generation - ESA Cloud_cci, Issue 1, Revision: 0, planned date of Issue: 06/2017. Available at: <http://www.esa-cloud-cci.org/?q=documentation>

RODCv1.0, Report on Orbital Drift Correction for AVHRR - ESA Cloud_cci, Issue 1, Revision: 0, planned date of Issue: 06/2017. Available at: <http://www.esa-cloud-cci.org/?q=documentation>

Rodgers, C.D. , 2000: Inverse methods for atmospheric sounding, World Scientific Publishing Pte Ltd, New York, USA.

Smith, D. L., Delderfield, J., Drummond, D., Edwards, T., Mutlow, C. T., Read, P. D., and Toplis, G. M.: Calibration of the AATSR Instrument, *Adv. Space Res.*, 28(1), 31--39, 2001.

Smith, D., Poulsen, C., and Latter, B.: Calibration status of the AATSR reflectance channels, 2008 ESA MERIS/(A)ATSR Workshop, 2008.

	Doc:		Cloud_cci_D2.1_ATBD_v6.2.doc		
	Date:		14 October 2019		
	Issue:	6	Revision:	2	Page 26

Stamnes K., Tsay S.C., Wiscombe W. and Jayaweera K., 1998: Numerically stable algorithm for discrete ordinate method radiative transfer in multiple scattering and emitting layered media, *Appl. Opt.*, 27, 2502-2509.

Stengel, M., Stapelberg, S., Sus, O., Schlundt, C., Poulsen, C., Thomas, G., Christensen, M., Carbajal Henken, C., Preusker, R., Fischer, J., Devasthale, A., Willén, U., Karlsson, K.-G., McGarragh, G. R., Proud, S., Povey, A. C., Grainger, D. G., Meirink, J. F., Feofilov, A., Bennartz, R., Bojanowski, J., and Hollmann, R.: Cloud property datasets retrieved from AVHRR, MODIS, AATSR and MERIS in the framework of the Cloud_cci project, *Earth Syst. Sci. Data Discuss.*, <https://doi.org/10.5194/essd-2017-48>, in review, **2017**.

Stengel, M., Schlundt, C., Stapelberg, S., Sus, O., Eliasson, S., Willén, U., and Meirink, J. F.: Comparing ERA-Interim clouds with satellite observations using a simplified satellite simulator, *Atmos. Chem. Phys. Discuss.*, <https://doi.org/10.5194/acp-2018-258>, in review, **2018**.

Stengel, M.; Stapelberg, S.; Sus, O.; Finkensieper, S.; Würzler, B.; Philipp, D.; Poulsen, C.; Christensen, M.; McGarragh, G.R. Cloud cci AVHRR-PM version 3.0 dataset: 35 yr climatology of global cloud and radiation properties. **2019**, in preparation. To be submitted to ESSD.


Stephens, G. L., Gabriel, P. M., and Partain, P. T. (2001). Parameterization of Atmospheric Radiative Transfer. Part I: Validity of Simple Models. *Journal of the Atmospheric Sciences*, 58(22):3391-3409.

Stubenrauch, C. J., A. G. Feofilov, S. E. Protopapadaki, R. Armante, 2017: Cloud climatologies from the InfraRed Sounders AIRS and IASI: Strengths, Weaknesses and Applications In preparation for submission to ACPD

Sus, O., Stengel, M., Stapelberg, S., McGarragh, G., Poulsen, C., Povey, A. C., Schlundt, C., Thomas, G., Christensen, M., Proud, S., Jerg, M., Grainger, R., and Hollmann, R.: The Community Cloud retrieval for CLimate (CC4CL) - Part 1: A framework applied to multiple satellite imaging sensors, *Atmos. Meas. Tech.*, 11, 3373-3396, <https://doi.org/10.5194/amt-11-3373-2018>, **2018**.


Walther, A. and Heidinger, A.K., 2012. Implementation of the daytime cloud optical and microphysical properties algorithm (DCOMP) in PATMOS-x. *Journal of Applied Meteorology and Climatology*, 51(7), pp.1371-1390.

Watts P.D., Mutlow C.T., Baran A.J. and Zavody A.M., 1998: Study on cloud properties derived from Meteosat Second Generation Observations. Eumetsat Report, http://www.eumetsat.de/en/area2/publications/rep_cloud.pdf.

	Doc:	Cloud_cci_D2.1_ATBD_v6.2.doc			
	Date:	14 October 2019			
	Issue:	6	Revision:	2	Page 27

6. Glossary

AMSR-E	Advanced Microwave Scanning Radiometer-EOS
AATSR	Advanced Along Track Scanning Radiometer
AM	Ante Meridiem
AVHRR	Advanced Very High Resolution Radiometer
BRDF	Bidirectional Reflectance Distribution Function
BT	Brightness Temperature
Calipso	Cloud-Aerosol Lidar and Infrared Pathfinder Satellite Observation
CFC	Cloud Fractional Coverage
CLOUDSAT	Cloud-Aerosol Lidar and Infrared Pathfinder Satellite Observations
CM SAF	EUMETSAT Satellite Application Facility on Climate Monitoring
CMUG	Climate Modelling User Group
CPH	Cloud Phase
COT	Cloud Optical Thickness
CTH	Cloud Top Height
CTP	Cloud Top Pressure
CTT	Cloud Top Temperature
DISORT	Discrete Ordinates Radiative Transfer
ECMWF	European Centre for Medium-Range Weather Forecasts
ECV	Essential Climate Variable
ENVISAT	Environmental Satellite
EOS	Earth Observing System
ESA	European Space Agency
FAME-C	FUB AATSR MERIS Cloud retrieval algorithm
FCDR	Fundamental Climate Data Record
GAC	Global Area Coverage - globally available AVHRR dataset with reduced resolution (4 km).
GSICS	Global Space-based Inter-Calibration System
GCOS	Global Climate Observing System
GEWEX	Global Energy and Water Cycle Experiment
JCH	Joint Cloud property Histogram
ISCCP	International Satellite Cloud Climatology Project
IWP	Ice Water Path
K	Kelvin

	Doc:		Cloud_cci_D2.1_ATBD_v6.2.doc		
	Date:		14 October 2019		
	Issue:	6	Revision:	2	Page 28

KNMI	Koninklijk Nederlands Meteorologisch Instituut
LUT	Look-up Table
LWP	Liquid Water Path
MERIS	Medium Resolution Imaging Spectrometer
MetOp	Meteorological Operational Satellite
MODIS	Moderate Resolution Imaging Spectroradiometer
MOMO	Matrix Operator Model
NASA	National Aeronautics and Space Administration
NCDC	National Climatic Data Center
NSIDC	National Snow and Ice Data Center
NOAA	National Oceanic & Atmospheric Administration
OLCI	Ocean Land Colour Instrument
ORAC	Oxford RAL Aerosol and Cloud Algorithm
PATMOS-x	AVHRR Pathfinder Atmospheres - Extended
PM	Post Meridiem
CER	Effective Radius
RTTOV	Radiative Transfer for (A)TOVS
SEVIRI	Spinning Enhanced Visible and Infrared Imager
SNO	Simultaneous Nadir Overpass
SMHI	Swedish Meteorological and Hydrological Institute
SLSTR	Sea and Land Surface Temperature Radiometer
TCDR	Thematic Climate Data Record
TOA	Top Of Atmosphere